ANL/MSD/CP--88817
CONF-951155--78

PROPERTIES VARIATION WITH COMPOSITION OF SINGLE-CRYSTAL $Pb(Zr_xTi_{1-x})O_3$ THIN FILMS PREPARED BY MOCVD*

C. M. Foster, G. R. Bai, Z. Li, and R. Jammy

Materials Science Division
Argonne National Laboratory, Argonne, IL 60439

L. A. Wills and R. Hiskes

Hewlett Packard Laboratories
Hewlett-Packard Company
3500 Deer Creek Road
Palo Alto, CA 94304

December 1995

DISCLAIMER

To be presented at the Materials Research Society 1995 Fall Meeting, Symposium G: "Epitaxial Oxide Thin Films II," Boston, MA, November 27-December 1, 1995.

*Work supported by the U.S. Department of Energy, Basic Energy Sciences-Materials Sciences, under contract #W-31-109-ENG-38 and under a joint CRADA with Hewlett-Packard Company #C9301701.

Properties Variation with Composition of Single-Crystal $Pb(Zr_xTi_{1-x})O_3$ Thin Films Prepared by MOCVD

C. M. Foster, G.-R. Bai, Z. Li, and R. Jammy
Materials Science Division, Argonne National Laboratory, 9700 S. Cass Avenue, Argonne, IL 60439

L. A. Wills and R. Hiskes
Hewlett Packard Laboratories, Hewlett-Packard Company, 3500 Deer Creek Road, Palo Alto, CA 94304

ABSTRACT

Single-crystal thin films covering the full compositional range of $Pb(Zr_xTi_{1-x})O_3$ (PZT) $0 \leq x \leq 1$ have been deposited by metal-organic chemical vapor deposition (MOCVD). The films were grown on epitaxial, RF-sputter-deposited $SrRuO_3$ thin film electrodes on (001) $SrTiO_3$ substrates. X-ray diffraction (XRD), energy-dispersive electron spectroscopy (EDS) and optical waveguiding were used to characterize the crystalline structure, composition, refractive index, and film thickness of the deposited films. We found that the PZT films were single-crystalline for all compositions exhibiting cube-on-cube epitaxy with the substrate with very high degrees of crystallinity and orientation. We report the systematic variations in the optical, dielectric, polarization, and transport properties as a function of composition and the epitaxy-induced modifications in the solid-solution phase diagram of this system. These films exhibited electronic properties which showed clear systematic variations with composition. High values of remnant polarization (30-55 $\mu C/cm^2$) were observed at all ferroelectric compositions. Unlike previous studies, the dielectric constant exhibited a clear dependence on composition with values ranging from 225-650. The coercive fields decreased with increasing Zr concentration to a minimum of 20 kV/cm at the (70/30) composition. In addition, these films exhibited both high resistivity and dielectric-breakdown strength (~10^{13} Ω-cm at 100 kV/cm and >300 kV/cm, respectively) without any compensative doping.

INTRODUCTION

The synthesis of thin films of the lead-based ferroelectrics, $Pb(Zr_xTi_{1-x})O_3$ (PZT), $(Pb_{1-x}La_x)(Zr_yTi_{1-y})O_3$ (PLZT), etc., using a variety of techniques (e. g., sol-gel, sputtering, laser ablation, MOCVD) and the resulting properties of the films have been studied extensively [1]. Current interest in ferroelectric thin films results from the numerous potential applications for these materials which utilize the unique dielectric, pyroelectric, electro-optic, acousto-optic, and piezo-electric properties of ferroelectrics materials [1]. For many applications, such as non-volatile dynamic random access memory (DRAM) or electro-optic waveguide modulators, a highly textured microstructure is preferable or essential. Ferroelectric film deposition using

MOCVD has been widely reported and has been shown to be able to produce film microstructures from random polycrystalline to highly epitaxial [2].

There have been two previous reports on the deposition of highly-oriented PZT films over a wide range of composition using MOCVD [3-4]. Braun et. al. [3], covered the full compositional range with films deposited on sapphire (1-102); However, no underlying conductive electrode was used; consequently, no detailed or systematic study of film properties was reported. Sakashita et. al. [4], deposited films on (001)-textured Pt layers RF-sputter deposited on MgO(001) substrates. However, this study did not include Zr-rich compositions and the measured electrical properties of the films did not show the systematic variations with composition as expected from the extensive literature on ceramic materials [5].

We have systematically studied the effects of gas phase composition, substrate materials, substrate orientation, and deposition temperature on the phase, composition, crystallinity, morphology and domain structure of epitaxial thin films of $PbTiO_3$ [6-8]. In addition, we have discussed the effects of the choice of substrate material on the crystallinity, microstructure, domain formation, defect structure and optical properties of $PbTiO_3$ thin films [9-10]. We have also previously published preliminary reports on the growth, characterization and properties of PZT thin films with specific compositions [11]. In this paper, we report the results of a systematic study of PZT thin films grown using MOCVD on epitaxial, RF-sputter-deposited $SrRuO_3$ thin film electrodes on (001) $SrTiO_3$ substrates. We present the necessary growth conditions for producing single-crystalline thin films at any specific composition. We also include the results of structural characterization, optical, dielectric, polarization, ferroelectric fatigue and electronic-transport properties, and dielectric-breakdown-strength determination.

EXPERIMENTAL

Epitaxial $SrRuO_3$ thin films were deposited on epitaxial-grade (001) $SrTiO_3$ substrates by 90° off-axis, RF magnetron sputtering at a growth pressure of 15 Pa and deposition temperature of 650°C. Sputter deposition commenced at a power of 60W and a Ar/O_2 flow rate of 120/80 sccm. The growth rate of the $SrRuO_3$ layers was estimated from RBS to be ~160Å per hour [12].

The PZT thin film depositions were carried out in a low pressure, horizontal, cold wall reactor with a resistive substrate heater. Tetraethyl lead, $Pb(C_2H_5)_4$, zirconium t-butoxide, $Zr(OC(CH_3)_3)_4$, and titanium isopropoxide, $Ti(OC_3H_7)_4$, (Morton International, Advanced Materials, Danvers, MA) were used as the metal ion precursors. Details of the reactor design and deposition methods have been previously reported[6-10]. The growth conditions for the $Pb(Zr_xTi_{1-x})O_3$ are shown in Table I. The different compositions across the phase diagram were obtained using different ratios of Ti and Zr carrier gas flow rates; however, a combined total carrier-gas flow rate of 60 sccm was maintained for all compositions.

For electrical measurement, a small portion of each film was etched away to expose the underlying electrode and Ag top electrodes were electron-beam

evaporated to form capacitor structures. The film thickness was measured using a surface profile obtained from a Dektak 3030 profilometer and independently determined using optical waveguiding. Surface roughness was investigated using scanning electron microscopy (SEM) and the film composition was determined using energy dispersive x-ray spectroscopy (EDS).

X-ray θ–2θ diffraction and θ–rocking spectra of the films were obtained using a Rigaku diffractometer and a 3 kW Cu K_α x-ray source. Prism-coupling waveguide experiments were performed with a Metricon 2010 Prism-Film coupler using a HeNe laser (632.8 nm); this system has been described elsewhere [13]. Ferroelectric hysteresis loops and ferroelectric fatigue measurements were obtained using a Radiant Technologies RT6000HVS test system. Electrical transport measurements (leakage current vs. time, resistance vs. voltage, and dielectric-breakdown strength) were measured using a Keithley 238 source measurement unit. Dielectric constant and loss tangent (1 kHz) was obtained using a HP4192A impedance analyzer.

Table I. Growth Conditions

Substrate temperature	700°C	
Reactor pressure	5-6 torr	
OM precursor temperature	$Ti(OC_3H_7)_4$ $Zr(OC(CH_3)_3)_4$ $Pb(C_2H_5)_4$	28-32 °C 28-32 °C 26-29 °C
OM precursor pressure	$Ti(OC_3H_7)_4$ $Zr(OC(CH_3)_3)_4$ $Pb(C_2H_5)_4$	80-100 torr 80 torr 400 torr
Flow rate of reactant gas (O_2)	300 sccm	
Flow rate of OM and carrier gas (N_2)	$Ti(OC_3H_7)_4$ $Zr(OC(CH_3)_3)_4$ $Pb(C_2H_5)_4$	0-60 sccm 0-60 sccm 35 sccm
Flow rate of background gas (N_2)	600 sccm	
Film thickness	0.2-1.0 μm	
Film growth rate	25-40Å/min.	
Substrates	$SrRuO_3/SrTiO_3$ (001)	

RESULTS AND DISCUSSION

To prepare PZT thin films with controlled composition using MOCVD, we first determined optimal growth conditions for the end compounds, $PbTiO_3$ and $PbZrO_3$. Under optimized conditions, we were able to grow single-crystalline $PbTiO_3$ and $PbZrO_3$ on $SrTiO_3$ (002) with excellent orientation (θ-rocking FWHM ≤ 0.4°), high values of refractive index (n_o~ 2.4607 for $PbZrO_3$, 2.6735 for $PbTiO_3$), and approximately equivalent growth rates (~35Å/min.). Of critical importance was that an identical carrier-gas flow rate for the Pb precursor was used for both $PbTiO_3$ and $PbZrO_3$. This greatly simplified the preparation of solid-solution compositions,

which were obtained using a constant combined Zr + Ti carrier gas flow rate of 60 sccm and simply varying the carrier-gas-flow-rate ratio, Ti/Zr. This produced a nearly linear relation between Ti/Zr and actual film composition determined by EDS. These growth conditions are specified in Table I.

Using these growth conditions for PZT, the films produced were pure perovskite phase with a single-crystalline structure. SEM images of the film surfaces showed an extremely smooth and featureless morphology (to $5x10^5$ magnification). In contrast to films grown on Pt coated MgO [4] that exhibited clear 1 X 1 μm grains, no indication of grain structure or grain boundaries could be observed for any composition. TEM micrographs published previously [11] have shown that the microstructure of these films is single-crystalline, with atomically sharp interfaces at the PZT/$SrRuO_3$ boundary. The thickness of the $SrRuO_3$ buffer layers was ~35-40 nm, as determined by RBS and TEM measurements. These studies have determined that the primary structural defects in the films are interfacial misfit dislocations, threading dislocations, and ferroelectric domains arising from the paraelectric-to-ferroelectric phase transformation.

Shown in Fig. 1 are results two-circle XRD for films of $Pb(Zr_xTi_{1-x})O_3$ of various compositions grown on epitaxial $SrRuO_3$(001) buffered $SrTiO_3$(001): x = 0.0, 0.15, 0.35, 0.49, 0.56, 0.70, 0.92, and 1.0. The data indicate that the films are (001) oriented for tetragonal compositions (x = 0.0, 0.15, 0.35, and 0.49), (012) oriented for rhombohedral compositions (x = 0.56, 0.70, and 0.92) and (002) oriented for the orthorhombic composition (x = 1.0). These orientations are related distortions of the same initial pseudo-cubic structure. This supports a cube-on-cube epitaxial relation of the growing film (in the cubic, paraelectric state) with that of the substrate for all compositions. This relation is preserved even as the substrate-film lattice mismatch worsens with increasing Zr concentration. The high-temperature cubic structure of the film then distorts upon cooling resulting in the orientations observed in Fig. 1. θ-rocking curves of the films exhibited FWHM of 0.2-0.6° for all compositions, showing that the films were highly oriented. In addition, the θ-rocking curves showed evidence that all the films contained domain structure [10]. For tetragonal compositions, the presence of off-specular PZT(100) reflections, resulting from 90° domain formation [10,11], could be observed. From integrated intensity ratios, we could determine that the films with tetragonal structure contained ~15-30% volume fraction of 90° domains.

The lattice constants of epitaxial $Pb(Zr_xTi_{1-x})O_3$ thin films grown on epitaxial $SrRuO_3$(001) buffered $SrTiO_3$(001) as a function of composition, x, are shown in Fig. 2a and compared to those of bulk PZT ceramics [14]. The lattice constants were determined from the 2θ values of the (002) and (200) reflections in XRD. While the lattice constants show a very similar trend to that of bulk material, there are several significant differences. First, for tetragonal materials, the *a*-axis lattice parameter is larger and the *c*-axis lattice parameter is smaller than that of bulk ceramics. Second,

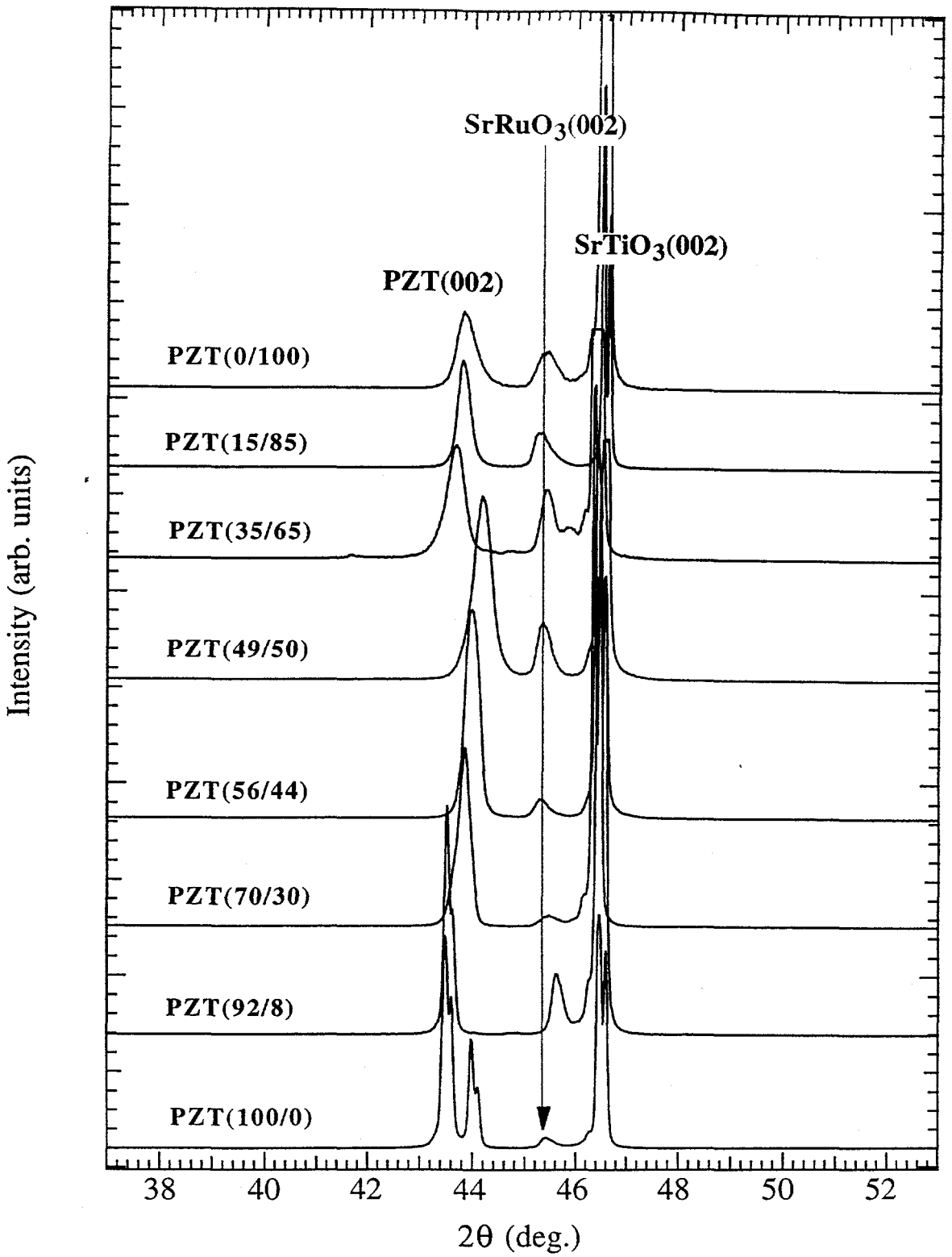

Figure 1. XRD patterns for epitaxial $Pb(Zr_xTi_{1-x})O_3$ thin films grown at 700°C on epitaxial $SrRuO_3(001)$ buffered $SrTiO_3(001)$ showing the systematic variation on lattice constants with composition. The films exhibited cube-on-cube epitaxial orientation with respect to the substrate.

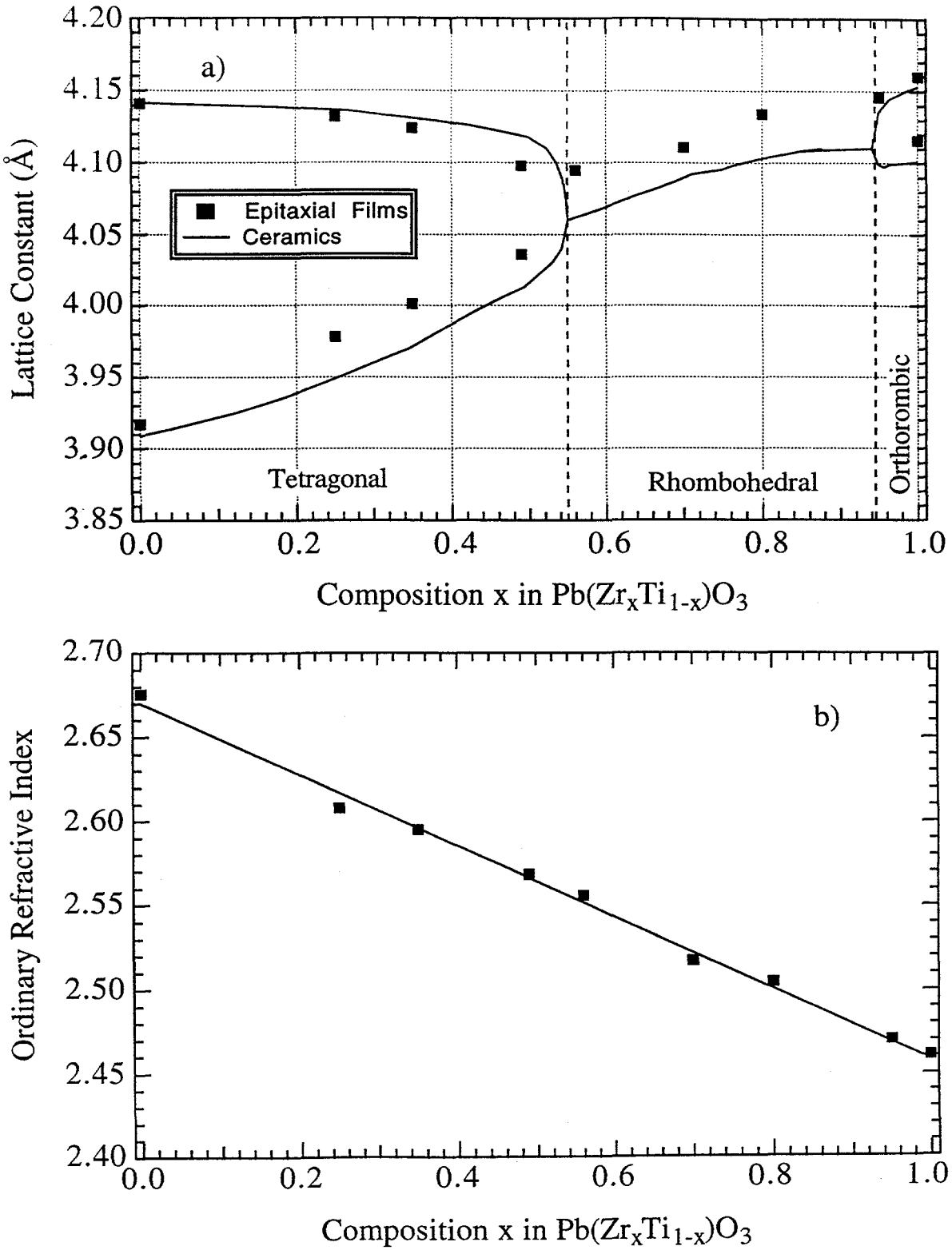

Figure 2. a) Lattice constants of epitaxial $Pb(Zr_xTi_{1-x})O_3$ thin films grown at 700°C on epitaxial $SrRuO_3(001)$ buffered $SrTiO_3(001)$ derived form XRD data as a function of composition. The solid lines are the lattice constants for ceramic materials [14]. b) Variation of the optical index of refraction (632.8 nm) with composition for epitaxial $Pb(Zr_xTi_{1-x})O_3$ thin films obtained by prism-coupled waveguide measurements.

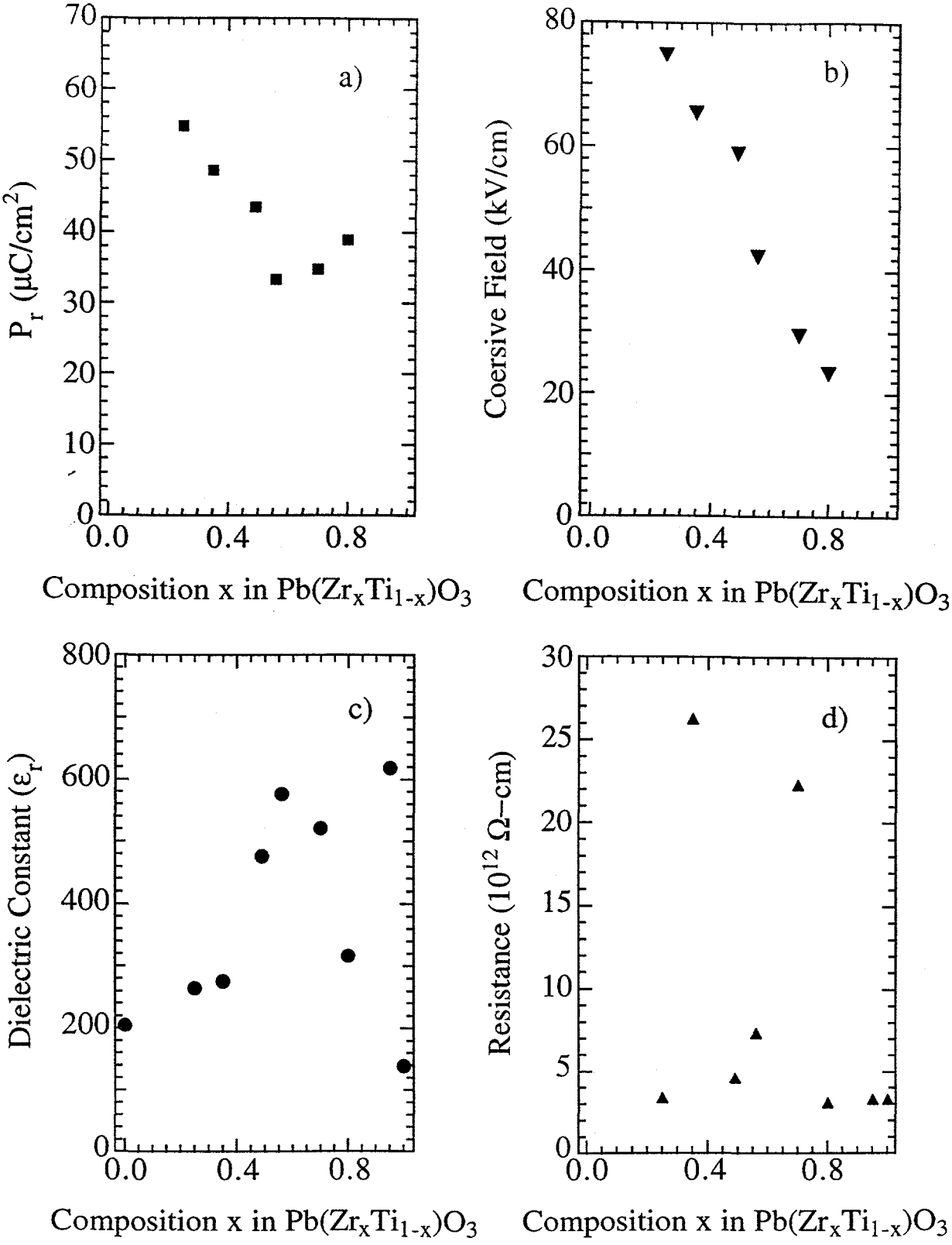

Figure 3. Variation of electronic properties with composition for $Pb(Zr_xTi_{1-x})O_3$ thin films grown at 700°C on epitaxial $SrRuO_3(001)$ buffered $SrTiO_3(001)$: a) remnant polarization, P_r, b) coercive field, E_c, c) dielectric constant, ε_r and d) electrical resistivity.

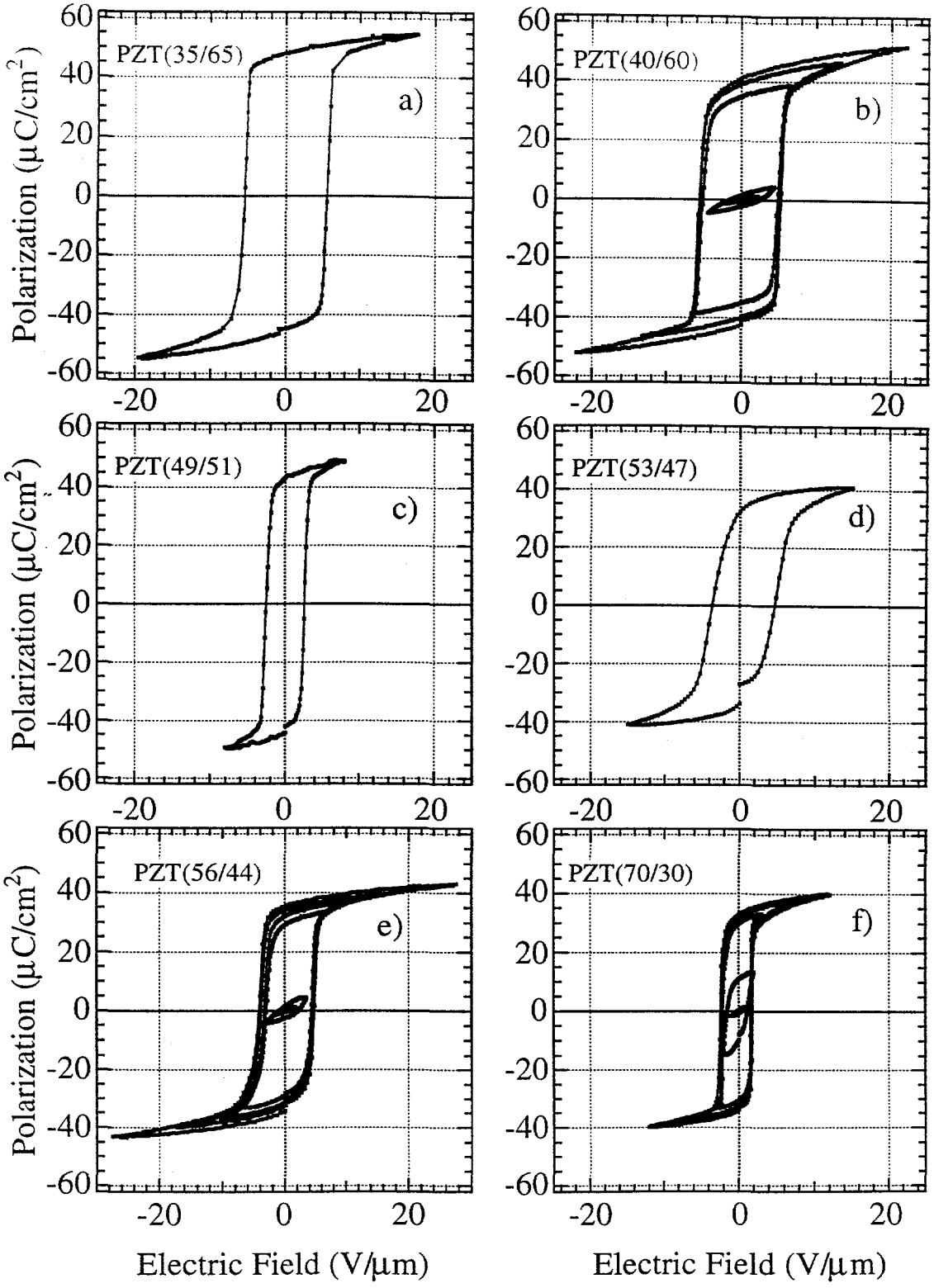

Figure 4. Ferroelectric hysteresis loops for various compositions of epitaxial $Pb(Zr_xTi_{1-x})O_3$ thin films grown at 700°C on epitaxial $SrRuO_3$ (001) buffered $SrTiO_3$ (001) substrates: x = a) 0.35, b) 0.40, c) 0.49, and d) 0.53, which were tetragonal structured, e) 0.56, and f) 0.70 which were rhombohedral structured.

the morphotropic phase boundary (x = 0.53 in ceramics [14]) is shifted to higher Ti content (x ~ 0.50) for films. Third, the *a*-axis lattice constant for all rhombohedral compositions is significantly smaller than those observed in bulk ceramics. Fourth, the phase boundary between the rhombohedral and orthorhombic phases is shifted to somewhat high Zr concentrations (x = 0.94) compared to that of bulk ceramics (x = 0.93) [14]. Fifth, the lattice constants for $PbZrO_3$ films are also larger than that of bulk ceramics. We attribute the increased compositional range of the rhombohedral-phase region to the larger component of shear-strain relaxation associated with structural twinning in the rhombohedral phase as opposed to twinning in the tetragonal or orthorhombic phases.

The refractive index for epitaxial $Pb(Zr_xTi_{1-x})O_3$ thin films grown on epitaxial $SrRuO_3(001)$ buffered $SrTiO_3(001)$ as a function of composition, x, are shown in Fig. 2b. The refractive index values represent an effective ordinary refractive index as determined by the pattern of the transverse-electric optical waveguide modes. The composition was determined by EDS analysis. The solid-line linear fit to the data, also shown in Fig. 2b, illustrates the linear dependence of the refractive index of the films with composition that is expected for a solid-solution system. To our knowledge, this is the first report of the compositional dependence of the refractive index of PZT. We have found that for PZT films of sufficient thickness (≥ 400 nm), the refractive index data in Fig. 2b provides a convenient and reasonably accurate (± 2-3%) method for quickly determining Zr/Ti composition.

In Fig. 3, we show the variation of some of the important electronic properties of epitaxial $Ag/Pb(Zr_xTi_{1-x})O_3/SrRuO_3(001)/SrTiO_3(001)$ capacitors stacks with composition, x. Figs. 3a and 3b show the compositional dependence of the remnant polarization (P_r) and coercive field (E_c), respectively. For $x < 0.30$ and $x > 0.80$, clean ferroelectric hysteresis loops were not observed due to high leakage currents. For $0.30 < x < 0.80$, the P_r values were in the range of 55-32 $\mu C/cm^2$ and showed a clear dependence on x with a minimum near the morphotropic boundary. E_c values exhibited a steep decline with increasing x, from 76 kV/cm at x = 0.30 to 21.5 kV/cm at x = 0.80. Compared to films prepared by sputtering [15] or pulsed laser deposition [16], the P_r values are higher and the E_c value are lower. In addition, both P_r and E_c exhibit compositional dependencies similar to bulk ceramics [5]. Figs. 3c shows the dependence of the relative dielectric constant (ε_r) as a function of composition. ε_r exhibits a peak near the morphotropic boundary and at the ferroelectric-antiferroelectric boundary similar to bulk ceramics. The dielectric loss, tan δ, was above 0.10 for $x < 0.20$. However, for $x \geq 0.20$, tan δ was 0.015-0.04. Fig. 3d, shows that for $x \geq 0.20$, the electrical resistivity (ρ) of the films is in the range of 10^{12}-10^{14} Ω-cm. The breakdown strength of the films was ≥300 kV/cm for all compositions.

Fig. 4 shows the P-E the hysteresis loops for $Pb(Zr_xTi_{1-x})O_3/SrRuO_3(001)$ $/SrTiO_3(001)$ films of various compositions: x = a) 0.35, b) 0.40, c) 0.49, and d) 0.53, which were tetragonal, e) 0.56, and f) 0.70 which were rhombohedral. The loop show that the films exhibit excellent ferroelectricity, square-shaped with large spontaneous polarization and low coercive fields.

In summary, single-crystal thin films covering the full compositional range of $Pb(Zr_xTi_{1-x})O_3$ (PZT) $0 \leq x \leq 1$ have been deposited by metal-organic chemical vapor deposition (MOCVD). The films were grown on epitaxial, RF-sputter-deposited $SrRuO_3$ thin film electrodes on (001) $SrTiO_3$ substrates. We showed the systematic variations in the optical, dielectric, polarization, and transport properties as a function of composition and the epitaxy-induced modifications in the solid-solution phase diagram of this system. High values of remnant polarization (30-55 $\mu C/cm^2$) were observed at all ferroelectric compositions. Unlike previous studies, the dielectric constant exhibited a clear dependence on composition with values ranging from 225-650. The coercive fields decreased with increasing Zr concentration to a minimum of 20 kV/cm at the (70/30) composition. In addition, these films exhibited both high resistivity and dielectric-breakdown strength (~10^{13} Ω-cm at 100 kV/cm and >300 kV/cm, respectively) without any compensative doping.

ACKNOWLEDGMENTS

This work was supported by the U. S. Department of Energy, Basic Energy Science-Materials Science under contract #W-31-109-ENG-38 under a joint CRADA with Hewlett-Packard Company #C9301701.

REFERENCES

1. For example see, Ferroelectric Thin Films III, ed. E. R. Myers, B. A. Tuttle, S. B. Desu, and P. K. Larsen, (Mat. Res. Soc. Symp. Proc. Vol. **310**, San Francisco, CA 1993).

2. C. J. Brierley, C. Trundle, L. Considine, R. W. Whatmore, and F. W. Ainger, Ferroelectrics **90**, 181 (1989); A. I. Kingon, K. Y. Hsieh, L. L. King, S. H. Rou, K. J. Backmann, and R. F. Davis, in Ferroelectric Thin Films, ed. by E. R. Myers and A. I. Kingon, (Mat. Res. Soc. Symp. Proc. Vol. **200**, Pittsburg, PA 1990); T. Katayama, M. Fuzimoto, M. Shimizu, and T. Shiosaki, Jpn. J. Appl. Phys. **30**, 2189 (1991).

3. W. Braun, B. S. Kwak, A. Erbil, J. D. Budai, and B. J. Wilkens, Appl. Phys. Lett. **63**, 467, (1993).

4. Yukio Sakashita, Toshiyuki Ono, Hideo Segawa, Kouji Tominaga, and Masaru Okada, J. Appl. Phys. **69**, 835 (1991).

5. For a review, see Yuhuan Xu, Ferroelectric Materials and Their Applications, North-Holland, New York, 1991, pp. 109-113.

6. G. R. Bai, H. L. M. Chang, H. K. Kim, C. M. Foster, and D. J. Lam, Appl. Phys. Lett. **64**, 408 (1992); Y. Gao, G. Bai, K. L. Merkle, Y. Shi, H. L. M. Chang, Z. Shen, and D. J. Lam, J. Mater. Res. **8**, 145 (1993).

7. G. R. Bai, H. L. M. Chang, C. M. Foster, Z. Shen, and D. J. Lam, J. Mater. Res. **9**, 156 (1994).

8. H. You, H. L. M. Chang, R. P. Chiarello, and D. J. Lam, in Heteroepitaxy of Dissimilar Materials, ed. by R. F. C. Ferrow, J. P. Harbison, P. S. Peercy, and A. Zangwill (Mat. Res. Soc. Symp. Proc. Vol. **221**, Pittsburg, PA 1990) p. 181.

9. C. M. Foster, Z. Li, G. R. Bai, H. You, D. Guo, and H. L. M. Chang, in Epitaxial Oxide Thin Films and Heterostructures, ed. D. K. Fork, J. M. Phillips, R. Ramesh, and R. M. Wolf, (Mat. Res. Soc. Symp. Proc. Vol. **341**, San Francisco, CA 1994).

10. C. M. Foster, Z. Li, M. Buckett, D. Miller, P. M. Baldo, L. E. Rehn, G. R. Bai, D. Guo, H. You and K. L. Merkle, J. Appl. Phys. **78**, 2607 (1995).

11. C. M. Foster, R. Csencsits, P. M. Baldo, G. R. Bai, Z. Li, L. E. Rehn, L. A. Wills and R. Hiskes in Smart Structures and Materials 1995, (Proc. of the SPIE Vol. **2441**. San Diego, CA 1995). C. M. Foster, R. Csencsits, P. M. Baldo, G. R. Bai, Z. Li, L. E. Rehn, L. A. Wills, R. Hiskes, D. Dimos and M. B. Sinclair, , in Ferroelectric Thin Films IV, ed. by R. Ramesh and B. Tuttle, (Mat. Res. Soc. Symp. Proc. Vol. **361**, Boston, MA 1994) pp. 307.

12. L. A. Wills and J. Amano, in Ferroelectric Thin Films IV, ed. by R. Ramesh and B. Tuttle, (Mat. Res. Soc. Symp. Proc. Vol. **361**, Boston, MA 1994).

13. C. M. Foster, S.-K. Chan, H. L. M. Chang, R. P. Chiarello, T. J. Zhang, J. Guo, and D. J. Lam, J. Appl. Phys. **73**, 7823 (1993).

14. G. Shirane and K. Suzuke, J. Phys. Soc. Jpn. **3**. 333 (1952).

15. T. Hase and T. Shiosaki, Jpn. J. Appl. Phys. **30**, 2159 (1991), T. Okamura, M. Adachi, T. Shiosaki and A. Kawabata, Jpn. J. Appl. Phys. **30**, 1034 (1991).

16. J. S. Horwitz, K. S. Grabowski, D. B. Chrisey, and R. E. Leuchtner, Appl. Phys. Lett **59**, 1565 (1991). R. Ramesh, B. Dutta, T. S. Ravi, J. Lee, T. Sands, and V. G. Keramidas, Appl. Phys. Lett. **64**, 1588 (1994).